Available online at www.sciencedirect.com
ScienceDirect
Expert Systems with Applications 36 (2009) 3562–3573
Expert Systems with Applications
www.elsevier.com/locate/eswa

Segmenting ideal morphologies of sewer pipe defects on CCTV images for automated diagnosis

Ming-Der Yang *, Tung-Ching Su

Department of Civil Engineering, National Chung Hsing University, 250, Kuo Kuang Road, Taichung 402, Taiwan

Abstract

Several literatures presented automated systems for detecting or classifying sewer pipe defects based on morphological features of pipe defects. In those automated systems, however, the morphologies of the darker center or some uncertain objects on CCTV images are also segmented and become noises while morphology-based pipe defect segmentation is implemented. In this paper, the morphology-based pipe defect segmentation is proposed and discussed to be an improved approach for automated diagnosis of pipe defects on CCTV images. The segmentation of pipe defect morphologies is first to implement an opening operation for gray-level CCTV images to distinguish pipe defects. Then, Otsu's technique is used to segment pipe defects by determining the optimal thresholds for gray-level CCTV images of opening operation. Based on the segmentation results of CCTV images, the ideal morphologies of four typical pipe defects are defined. If the segmented CCTV images match the definition of those ideal morphologies, the pipe defects on those CCTV images can be successfully identified by a radial basis network (RBN) based diagnostic system. As for the rest CCTV images failing to match the ideal morphologies, the failure causes was discussed so to suggest a regulation for imaging conditions, such as camera pose and light source, in order to obtain CCTV images for successful segmentation.

Keywords: CCTV; Image processing; Morphologies of pipe defects; Diagnostic system

1. Introduction

Sewage rehabilitation plays an important role during the maintenance of a sewer system, but is not easily processed due to the uncertainty of sewer pipe defects. Thus, worldwide engineers pay a great attention to plan proactive and preventive repair strategies than the traditional approach of passive sewage maintenance (Fenner, 2000; Yang & Su, 2007). Before undertaking sewer rehabilitation plan, needed are series steps of sewage rehabilitation planning including sewage inspection, diagnosis of sewer pipe defects, computation of structural condition grades, and determination of cost-effectiveness rehabilitation approaches (Yang & Su, 2006). Various tools or technologies such as closed circuit television (CCTV) cameras mounted on robots, ground piercing radar (GPR), sonar and infrared thermograph, are developed to assist engineers in sewage inspection (Fenner, 2000; Gokhale & Graham, 2004; Makar, 1999).

CCTV usually mounted on robot to be putted inside sewer pipes from a manhole and remote-controlled outside to acquire images of inner pipe is the most popular inspection tool because of its commercial availability (Makar, 1999; Mckim & Sinha, 1999). Acquired CCTV images from sewage inspection are used for diagnosing pipe defects to assess sewage structural conditions. However, during a sewage inspection work a great number of CCTV images are usually obtained so to be unsuitable for human diagnosis of pipe detects due to human's fatigue, subjectivity, time-consuming, and high cost (Mckim & Sinha, 1999; Moselhi & Shehab-Eldeen, 2000; Wirahadikusumah, Abraham, Iseley, & Prasanth, 1998).

Based on the morphological features of sewer pipe defects, several literatures presented automated systems

* Corresponding author. Tel.: +886 4 2284 0440x214; fax: +886 4 2286 2857.
E-mail address: mdyang@nchu.edu.tw (M.-D. Yang).

0957-4174/$ - see front matter © 2008 Elsevier Ltd. All rights reserved.
doi:10.1016/j.eswa.2008.02.006

for detection or diagnosis of sewer pipe defects (Moselhi & Shehab-Eldeen, 1999; Moselhi & Shehab-Eldeen, 2000; Shehab & Moselhi, 2005). Various sewer pipe defects on CCTV images are analyzed through different mathematical morphologies which are widely used for image analysis, smoothing, segmentation, edge detection, thinning, shape analysis and coding (Iyer & Sinha, 2005; Sinha & Fieguth, 2006). One of the automated systems used an innovative technology, called Sewer Pipe Scanner and Evaluation Technology (SSET), for obtaining images of the interior of sewer pipes to identify pipe defects (Mckim & Sinha, 1999). Even with an overall accuracy of the automated SSET system up to 90%, SSET comparative to CCTV is much less commercialized. Moreover, the quality and resolution of the CCTV image can compare favourably with the images of an SSET based system if CCTV is used state-of-the-art technology under ideal conditions (Mckim & Sinha, 1999).

One of the CCTV imaging problems is that the center area is always darker than the surrounding areas due to the fact that the lighting effect vanishes as the distance from the lighting source gets larger (Moselhi & Shehab-Eldeen, 2000). The shortage of lighting source causes the morphology of the mass of dark image region at the center of the original gray-level CCTV image being segmented, which increases the difficulty to segment a complete morphology of pipe defect. Moreover, open joint, joint displacements, and reductions in the cross-sectional area at the center of CCTV image are illuminated and would reflect back the beam of light due to the fact that these pipe defects tend to protrude from the surface of the pipe as oppose to other pipe defects such as crack and spalling. Moselhi and Shehab-Eldeen (2000) and Shehab and Moselhi (2005) proposed neural network technique-based automated systems for classification of sewer pipe defects and detection of sewage infiltration, respectively. First of all, an approach of morphology segmentation was applied to the CCTV images. Some of the segmented image regions belong to pipe defects, while others may belong to sewages or image background. However, this problem was not discussed in their literatures. Thus, the segmented image regions which belong to pipe defects usually need an expertise-based human diagnosis to be identified before an implementation of automated diagnosis.

In traditional inspection projects, a CCTV image is mostly diagnosed into one type of defect rather than multiple types of defects. Yang and Su (in press) presented a novel diagnostic system in which CCTV images were implemented by a two-dimensional discrete wavelet transform and computation of co-occurrence matrices to analyze the texture shown on the CCTV images. The features of pipe defects were straightly derived from the texture analyses of CCTV images so that the processes of feature extraction and classification of pipe defects on CCTV images can be thoroughly automated. However, the some inspection notations manually attached on the original CCTV images become harmful noises so to derive the extracted textural features of pipe defects with a linear non-separable relationship for the diagnosis system and to increase the difficulty of classification. This paper is aimed to discuss the related problems about morphology-based pipe defect segmentation on CCTV images as well as to propose an efficient approach to measure the morphological features of pipe defects from CCTV images. First of all, CCTV images are implemented a morphological segmentation using a combination of opening operation and Otsu's technique. Based on the segmentation results of CCTV images, the ideal morphologies of four typical pipe defects, such as broken pipe, crack, fracture, and open joint, are defined. Secondly, the CCTV images on which the pipe defects are segmented successfully are selected to be the experimental materials of a radial basis network (RBN) technique-based diagnostic system. Finally, the classification accuracy and utility of the diagnostic system are assessed. In this paper, the measured morphological features of pipe defects include area, major axis length, minor axis length, eccentricity, and ratio of major axis length to minor, which are defined in Appendix (Moselhi & Shehab-Eldeen, 2000; Shehab & Moselhi, 2005). The frame of this study is shown as in Fig. 1.

2. Methodology

Some morphological approaches based on set-theoretic concepts of shape have been successfully applied to many segmentation problems (Moselhi & Shehab-Eldeen, 1999; Moselhi & Shehab-Eldeen, 2000; Shehab & Moselhi, 2005; Sinha & Fieguth, 2006). In order to effectively segment out the pipe defects from CCTV images, morphology-based segmentation is adopted. Firstly, implemented is opening operation, in which erosion immediately followed by dilation is applied to a gray-level image using the same structuring element to distinguish the pipe defect on a CCTV image better (Gonzalez & Woods, 2002; Parker, 1997). Then, Otsu's technique is employed to find an optimal threshold for the opening operated gray-level image to segment the pipe defect because the technique is non-parametric, unsupervised, and automatic (Sinha & Fieguth, 2006). For those successfully segmented pipe defects, the morphological features are measured and transformed through a principal component analysis (PCA) into a substantially smaller set of uncorrelated variables representing most of the information in the original extracted morphological features in order to improve the accuracy of the RBN technique-based diagnostic system (Duda, Hart, & Stork, 2001; Wang & Paliwal, 2003; Widodo, Yang, & Han, 2007).

2.1. Opening operation

The light and dark portions of an image can be reshaped or morphed in various ways under a control of a structuring element which can be considered as a parameter to morphological operation (Sinha & Fieguth, 2006). Dilation

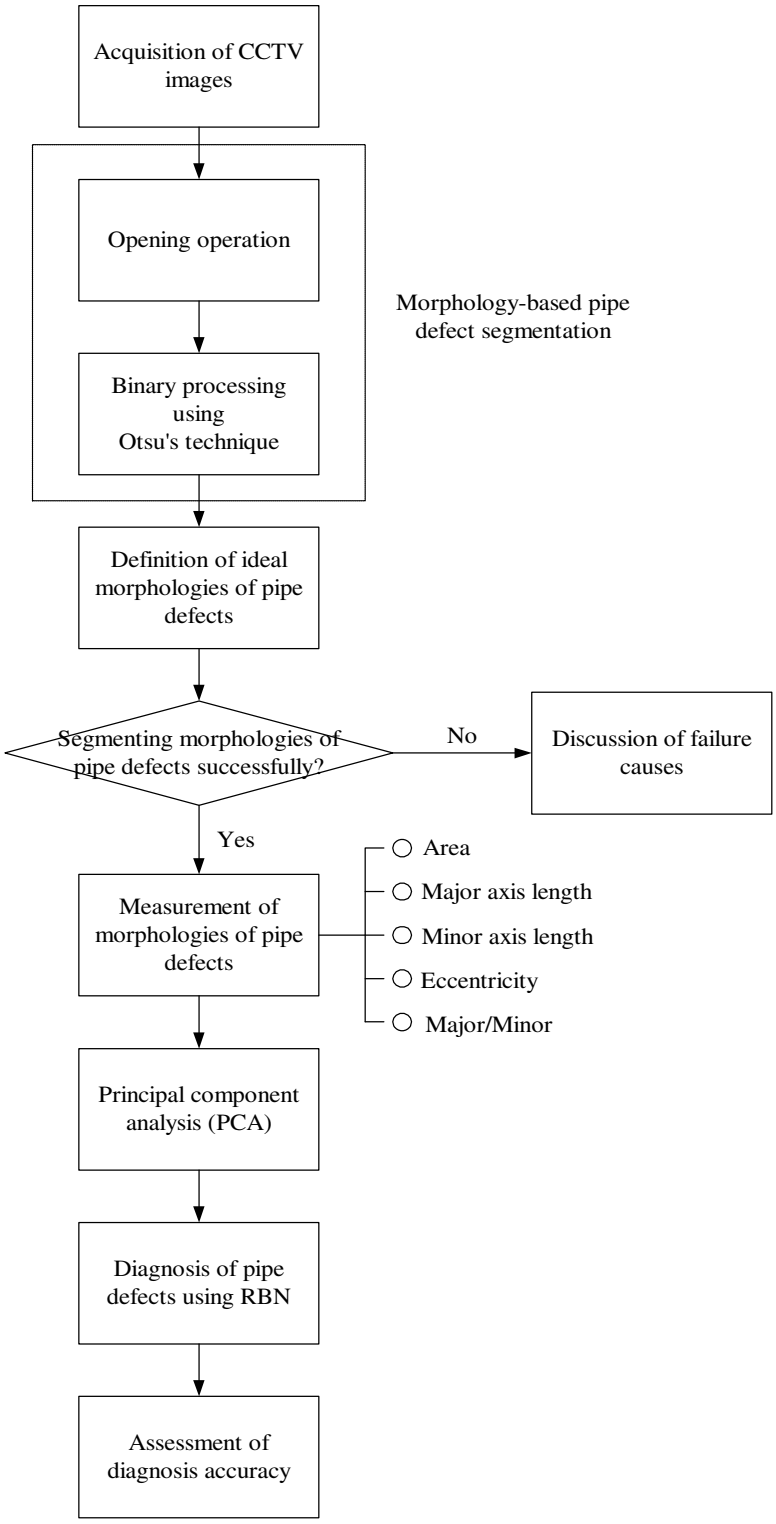

Fig. 1. Flowchart of a morphology-based pipe defect diagnosis.

and erosion are the two basic morphological operations (Dong, 1997). Sets A and B in $\mathbf{Z}^2$ are defined to represent a grey-level image consisting of pixels $p(x, y)$ and a structuring element, respectively:

$$A = \{(x,y)|p(x,y)\} \quad (1)$$

$$B = \{(x,y)|(x,y) \text{ in structuring element}\} \quad (2)$$

The dilation of A by B, denoted $A \oplus B$, is the union of all pixels in A surrounded by the shape of B and is defined as:

$$A \oplus B = \{a + b| \quad \text{for all } a \in A \text{ and } b \in B\} \quad (3)$$

Similarly, the erosion of A by B, denoted $A\Theta B$, removes all pixels within a "distance" B from the edge of A and is defined as

$$A\Theta B = \{a | b + a \in A \text{ for every } b \in B\} \quad (4)$$

The opening operation is defined as

$$A \circ B = (A\Theta B) \oplus B \quad (5)$$

The effect of opening operation is to remove image regions which are lightly relative to the structuring element while preserving image regions greater than structuring elements (Sinha & Fieguth, 2006).

2.2. Otsu's technique

In this paper, Otsu's technique is used to transform the opening operated gray-level CCTV images into the binary images for segmenting pipe defects. Otsu's technique, which is a thresholding method based discriminant analysis, determines the optimal thresholds for the opening operated gray-level images by maximizing the following measure of class separability (Yan, 1996):

$$D(T) = \frac{P_1(T)P_2(T)[m_1(T) - m_2(T)]^2}{P_1(T)\sigma_1^2(T) + P_2(T)\sigma_2^2(T)}, \quad (6)$$

where

$$P_1(T) = \sum_{z=0}^{T} h(z), \quad (7)$$

$$P_2(T) = \sum_{z=T+1}^{L-1} h(z) = 1 - P_1(T), \quad (8)$$

$$m_1(T) = \frac{1}{P_1(T)} \sum_{z=0}^{T} zh(z), \quad (9)$$

$$m_2(T) = \frac{1}{P_2(T)} \sum_{z=T+1}^{L-1} zh(z), \quad (10)$$

$$\sigma_1(T) = \frac{1}{P_1(T)} \sum_{z=0}^{T} [z - m_1(T)]^2 h(z), \quad (11)$$

$$\sigma_2(T) = \frac{1}{P_2(T)} \sum_{z=T+1}^{L-1} [z - m_2(T)]^2 h(z), \quad (12)$$

z is the grey-level of a pixel in the CCTV image and ranges from 0 through $L-1$, $h(z)$ is the normalized grey-level histogram of the CCTV image. By maximizing the criterion function in Eq. (6), the means of the light and dark image regions can be separated as well as possible and the variances of the two image regions can be minimized.

2.3. Principal component analysis (PCA)

PCA can be regarded as a classical method of multivariate statistical analysis for reducing the dimension of the original sets of data (Lillesand & Kiefer, 2000; Polat & Güneş, 2007; Widodo et al., 2007). A small set of uncorrelated variables derived from a transformation of PCA can be much more easily discriminated than an original lager set of correlated variables. Thus, this data compression technique has been widely applied to many fields including cluster analysis, regression, data compression and pattern recognition (Widodo et al., 2007).

At first, the d-dimensional mean vector $\boldsymbol{\mu}$ and $d \times d$ covariance matrix $\mathbf{M}$ are computed for the original set of morphological features of pipe defects $\mathbf{P}$. Then, the eigenvector $\mathbf{x} = \mathbf{e}_i$ $(i = 1, \ldots, d)$ and associated eigenvalue $\lambda = \lambda_i$ are computed using the following linear equation

$$\mathbf{M}\mathbf{x} = \lambda\mathbf{x} \quad (13)$$

for eigenvalue λ, which can be rewritten

$$(\mathbf{M} - \lambda\mathbf{I})\mathbf{x} = 0, \quad (14)$$

where $\mathbf{I}$ is the identity matrix and 0 is a zero vector. Those d eigenvectors are sorted by their largest eigenvalue, in which the first k eigenvectors are remained, and k is the inherent dimensionality of the subspace representing the most information in the original set of morphological features of pipe defects while the remaining $d-k$ dimensions generally contain noise (Duda et al., 2001). In common, there are just a few eigenvectors left for further pipe defect classification. Next, a $d \times k$ matrix $\mathbf{A}$, whose columns consist of the k eigenvectors, is formed. The representation of data by principal components consists of projecting the data onto the k-dimensional subspace according to

$$\mathbf{P}^t = \mathbf{A}^t(\mathbf{P} - \boldsymbol{\mu}). \quad (15)$$

2.4. Radial basis network (RBN) based classification approach

Currently, back-propagation neural network (BPN), radial basis network (RBN), and support vector machine (SVM) are the three commonly used neural networks (Liao, Fang, & Nuttle, 2004; Yang & Su, in press). Yang and Su (in press) employed these three neural networks to diagnose pipe defects based on textural features on CCTV images. The testing results indicate that BPN needs the longest computation time but with the lowest accuracy. SVM and RBN have better classification accuracy, but SVM needs to determine the best parameters a prior within the kernel functions based on heuristics at present (Seo, 2007; Yang & Su, in press). Thus, this paper employs the RBN technique to diagnose pipe defects based on their morphological features on CCTV images.

RBN is designed based on an unsupervised learning and a supervised learning (Zhang, Jiang, & Kamel, 2005). At the stage of unsupervised learning, clustering algorithm is used to divide all training samples of pipe defects s into subsets. The number of subsets is set as the number of neurons in the hidden layer of RBN. The characteristic of the training samples in each subset can be described by radial basis functions (G_j), one of activation functions, as (Hwang & Bang, 1997):

$$G_j = \begin{cases} \exp\left\{\frac{-\|s-c_j\|^2}{2\sigma_j^2}\right\}, & j = 1, 2, \ldots, n_H, \\ 1 & j = 0 \text{ (bais neuron)}, \end{cases} \quad (16)$$

where c_j and σ_j are the center and covariance matrix of each hidden neuron, respectively, which can be determined by clustering; $\|\cdot\|$ denotes the Euclidean distance; n_H represents the number of the hidden neurons. At the stage of supervised learning, a linear weighted sum between the hidden and output layers is computed as

$$z_l = \sum_{j=0}^{n_H} G_j w_{lj} \tag{17}$$

where l denotes the c classes of pipe defects; z_l is a linear weighted sum of the outputs of the hidden neurons; optimal w_{kl} is the solution of this set of linear equations by feed-forward calculation (Han & Xi, 2004; Liao et al., 2004; Zhang et al., 2005). A pipe defect pattern is fed into the trained RBN to be assigned into a certain class of pipe defect, so the output vector also has a dimension of $c \times n$ if n pipe defect patterns are recognized. Within an output vector, the lth element as a maximum z_l represents that this CCTV image is diagnosed as the lth pipe defect pattern.

3. Experimental materials

A sewer sub-system (called system G) at the 9th district of Taichung City, which is the largest city in the central Taiwan, is selected as the study case. The sewer system was made in Vitrified Clay Pipe (VCP) and built a decade ago. A CCTV inspection work by manual interpretation was implemented in 2003 for a reference of rehabilitation prior to a house-connecting construction, and there were 291 CCTV inspection images including 107 samples of open joint, 112 samples of crack, 16 samples of broken pipe, and 56 samples of fracture. The detail of system G

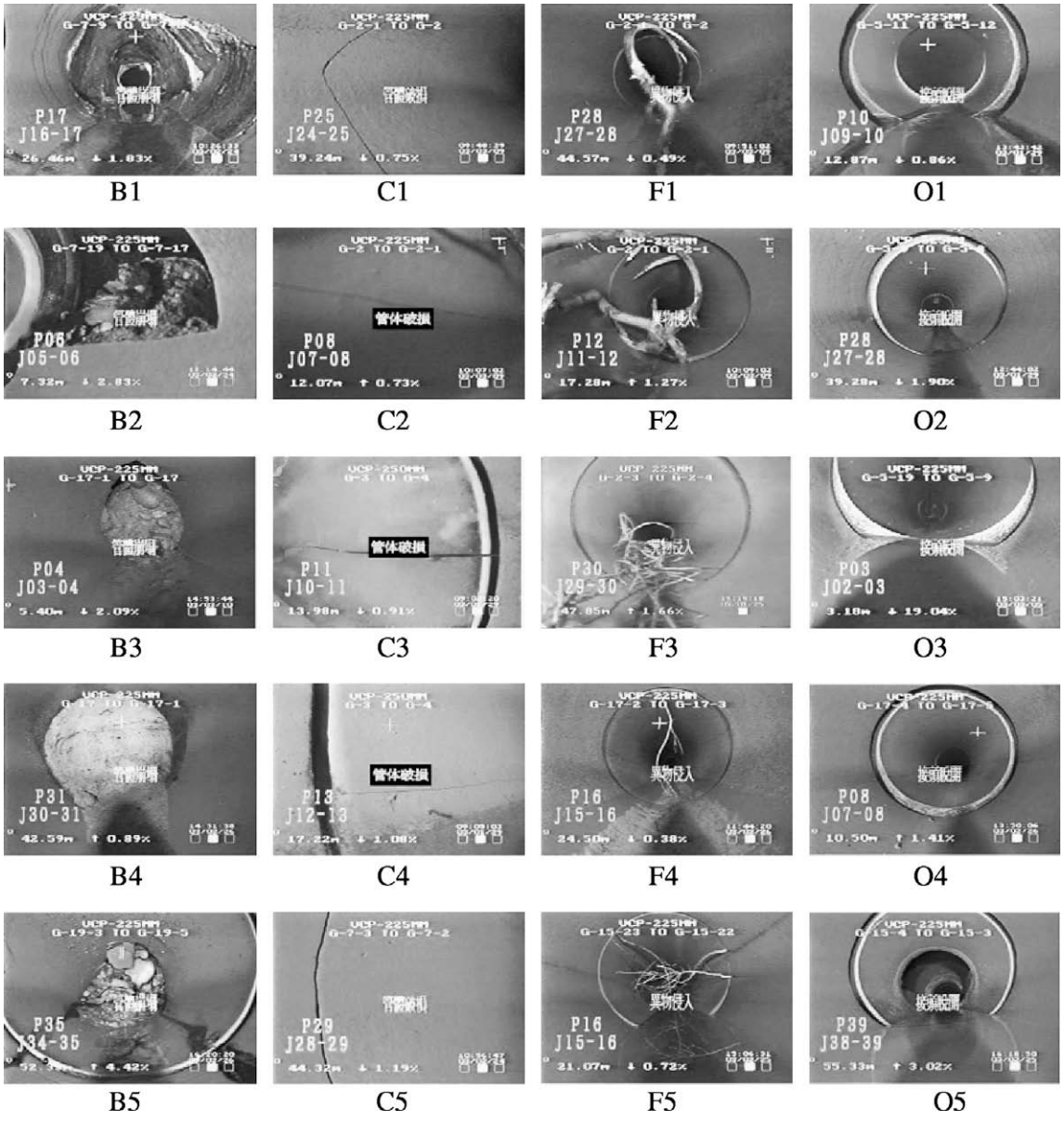

Fig. 2. CCTV images of pipe defect samples.

can be checked in Yang and Su's (in press). Open joint, crack, broken pipe, and fracture are the four typical pipe defects found in the inspection work, and each frame of CCTV image was only used to record one type of pipe defect. In this paper, each type of pipe defect is given five CCTV image samples for pipe defect segmentation due to their natural shape irregularities and the complex imaging environment (see Fig. 2). The alphabets, B, C, F, and O, represent broken pipe, crack, fracture, and open joint, respectively.

4. Results and discussion

4.1. Opening operation

In Fig. 2 manmade notations of inspection attributes attached directly on the acquired gray-level CCTV images can be discovered. During the morphology-based pipe defect segmentation, the utility of opening operation is expected not only to smooth the shapes of the notations but also to remain the original shapes of the pipe defects. In this paper, a disk structuring element of varying radius r and a rectangle structuring element of varying width w and a fixed length $l = 5$ were adopted in the test of an opening operation, and the illustrations of the two structuring elements can be referred in MATLAB 6.5 or more advanced visions. The gray-level CCTV image C1 in Fig. 2 was selected to be the testing image. The testing results of opening operation shown in Figs. 3 and 4 reveal that the larger the size of the structuring element is the better the performance of smoothing the shapes of the notations. Moreover, the disk structuring element of radius $r = 4$ or 5 comparative to the rectangle structuring element of width $w = 4$ or 5 and a fixed length $l = 5$ gives a better smoothing effect. However, if the size of the structuring element is too large, the original shape of object will be clearly deformed (Jang & Chin, 1998). Thus, the disk structuring element of radius $r = 4$ is employed in this research.

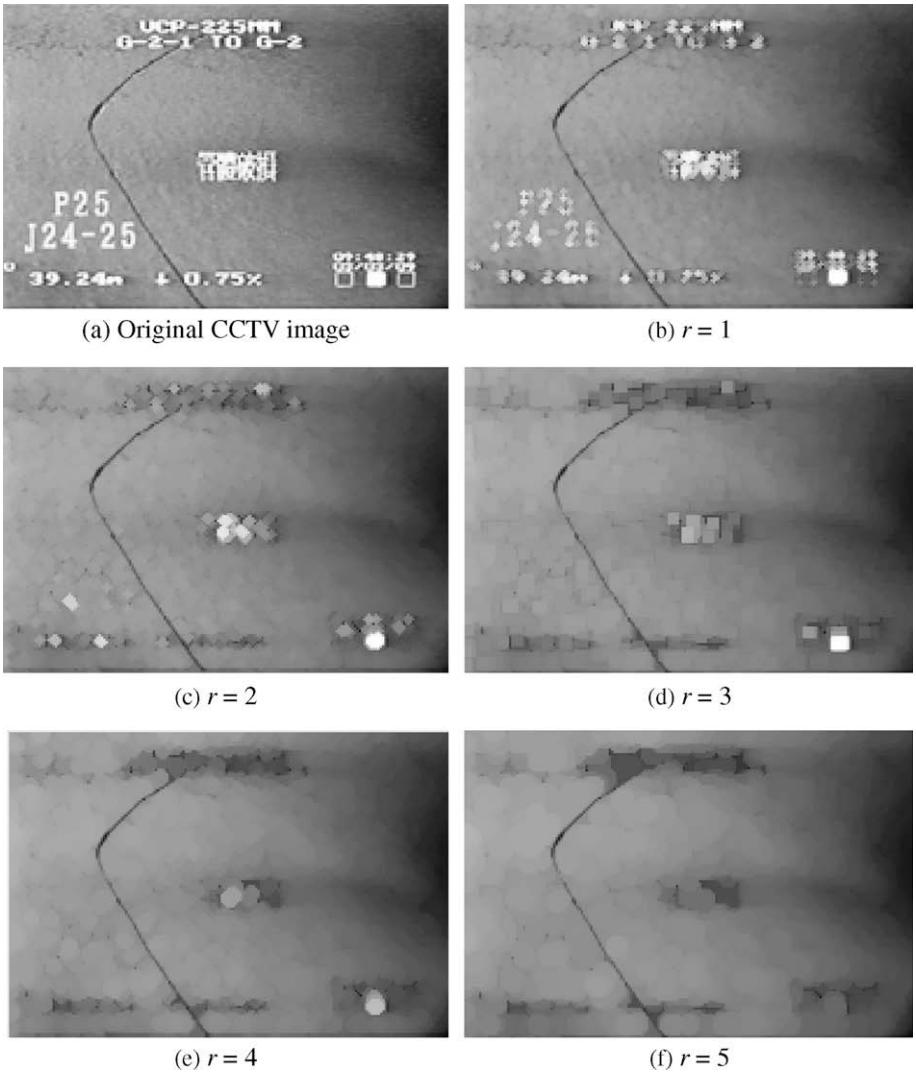

(a) Original CCTV image (b) $r = 1$

(c) $r = 2$ (d) $r = 3$

(e) $r = 4$ (f) $r = 5$

Fig. 3. Testing results of opening operation using a disk structuring element of varying radius r.

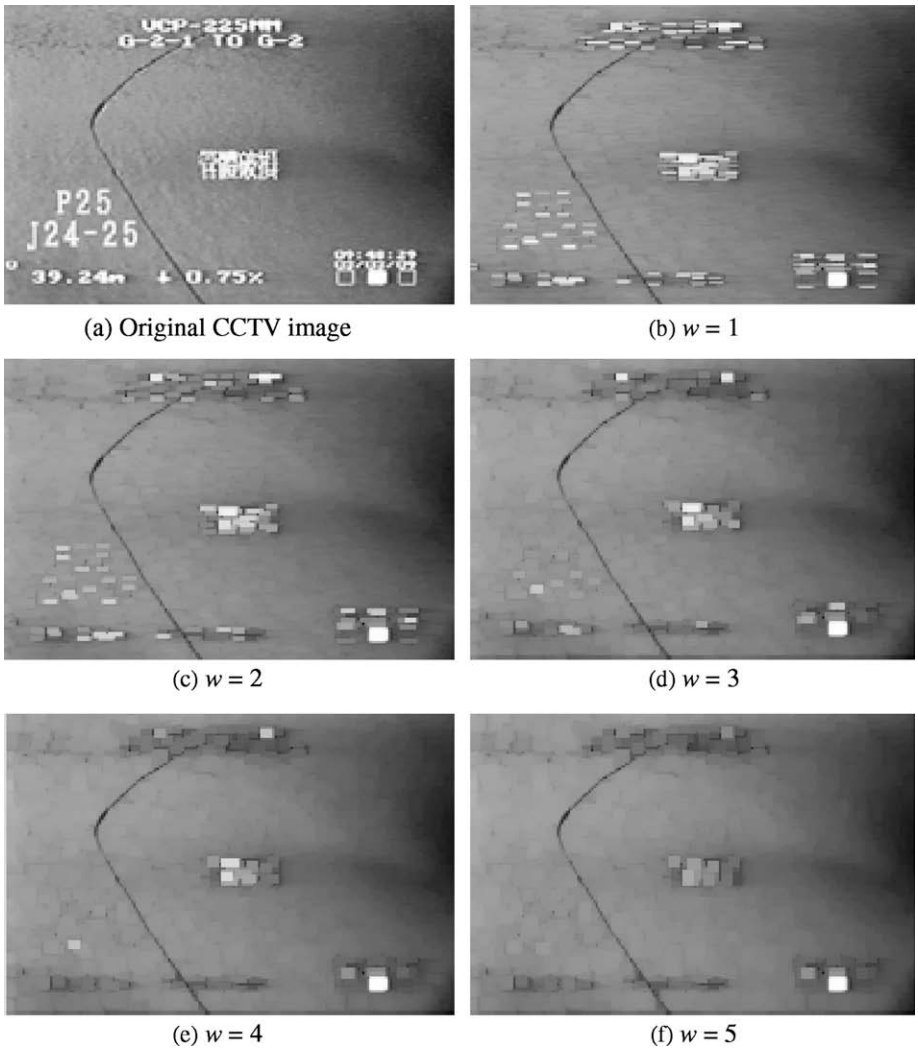

(a) Original CCTV image (b) $w = 1$

(c) $w = 2$ (d) $w = 3$

(e) $w = 4$ (f) $w = 5$

Fig. 4. Testing results of opening operation using a rectangle structuring element of varying width w and fixed length $l = 5$.

4.2. Morphology segmentation of pipe defects

In Fig. 2, debris and roots are the typical characteristics of broken pipe and fracture, respectively, with irregular shapes compared to crack and open joint. Cracks can be simply classified into circumferential crack and longitudinal crack (Water Research Centre, 1994). The shapes of open joint look like single circle or concentric circles. It can be found that the line of sight of camera was parallel to the centroid line of sewer pipe to acquire the gray-level CCTV images of fracture and open joint (see Fig. 2). As being mentioned before, the centers of those gray-level CCTV images are always darker than their surrounding areas. Similar with the segmentation results of Shehab and Moselhi (2005), both the segmented binary images of fracture and open joint in Fig. 5 show that the morphologies of the masses of dark image regions on the centers of the original gray-level CCTV images were segmented as the white image regions while a morphology segmentation of pipe defect was implemented. Thus, it is necessary but time-consuming for each segmented binary image to identify pipe defects in the bright image regions.

Most of the segmented binary images of open joint in Fig. 5 show that the morphologies of the sewages as well as those of the masses of dark image regions at the centers of the original gray-level CCTV images were clearly segmented. However, the segmented open joints usually accompanied with wastewater or/and the masses of dark image regions at the centers of the original gray-level CCTV images so to cause a difficulty to segment a complete morphology of open joint from an original gray-level CCTV image. To efficiently measure the morphological features of pipe defects from the segmented binary images, this paper gives a novel morphological definition for each type of pipe defect according to the segmentation results in Fig. 5. Fig. 6 presents the ideal morphologies of pipe defects by characterizing broken pipe, crack, fracture, and open joint as a white circle, an irregular white line, several irregular black lines within a white keyhole, and a white keyhole capped a white arc, respectively. The white

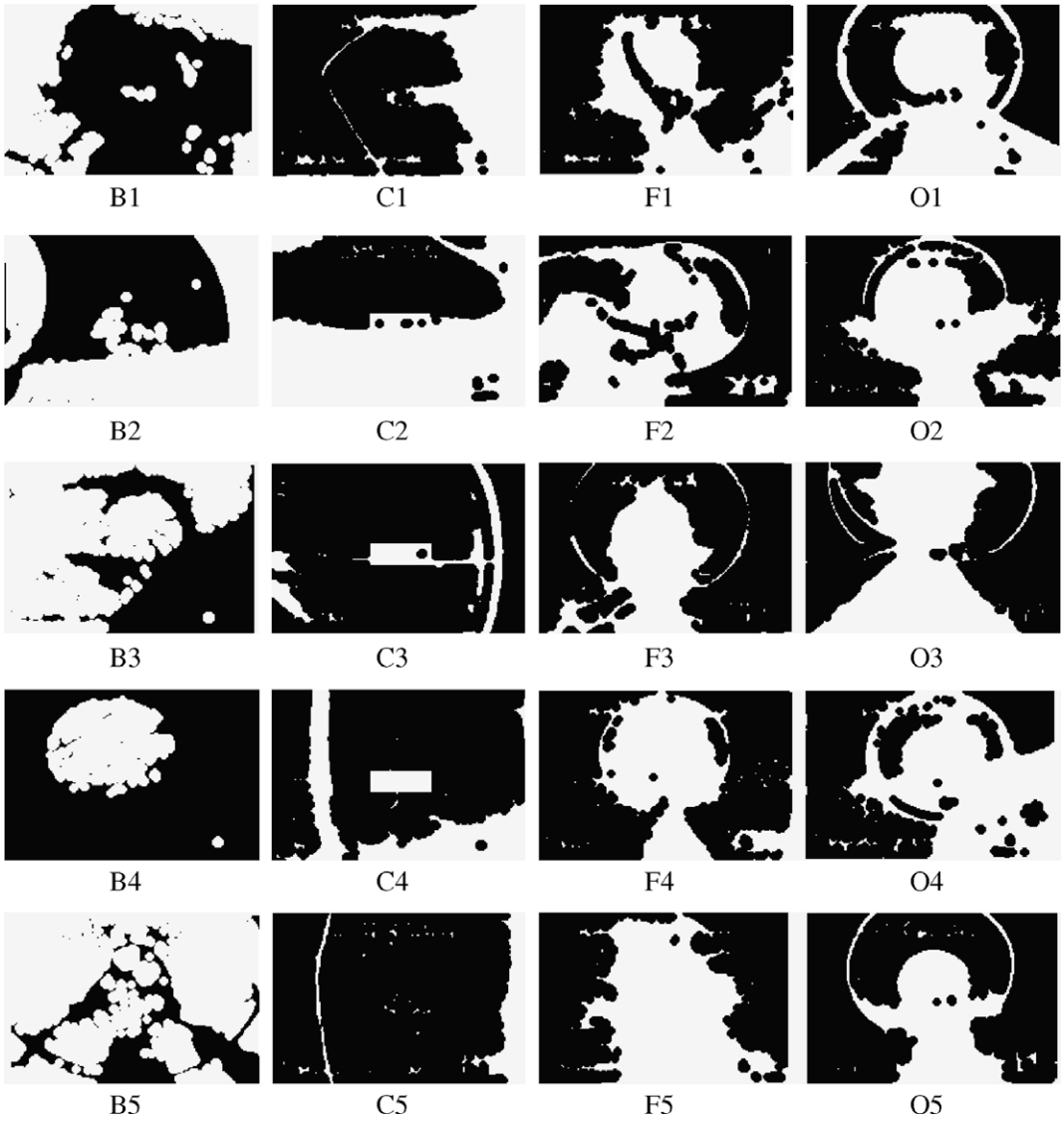

Fig. 5. Segmented binary images of pipe defects of the training set.

keyhole image region can be regarded as a combination of a white circle image region resulting from a segmentation of a mass of dark image region at the center of CCTV image and a white trapezoid image region resulting from a segmentation of sewages within pipes. Assuming collapsed debris blockading entire sewer pipes, there is no white trapezoid image region appearing on the typical illustration of the ideal morphology of broken pipe.

4.3. Failure causes and resolution of ideal morphology segmentation of pipe defects

The gray-level CCTV images of fracture in Fig. 2 show that the roots and the surrounding areas of the CCTV images are much lighter than the centers of the CCTV images. However, in Fig. 5 the segmented binary images F3, F4, and F5 show that the morphologies of the thin roots can not be effectively segmented so to result in a failure of measuring their morphological features. In Fig. 2, the reflectance light by debris appearing on the gray-level CCTV images of broken pipe affected the segmented morphologies of broken pipe. If the reflected light by debris is much stronger than that by surrounding pipe wall, the morphology of broken pipe can be completely segmented that can be revealed by comparing the binary image B4 in Fig. 5. In addition, compared to those of crack and open joint, the gray-level CCTV images of broken pipe seem to have locally obvious textures caused by the debris. Therefore, the segmented binary images of broken pipe in Fig. 5 show the morphologies of the debris in several white image regions that would increase the difficulty of automated measuring the morphological features of broken pipe.

In Fig. 2, the open joints reflect but the cracks absorb the exposing light from the CCTV platform. Both the cracks and open joints can be efficiently segmented from the original gray-level CCTV images. In other words, the light reflected back by pipe defects would not interfere a

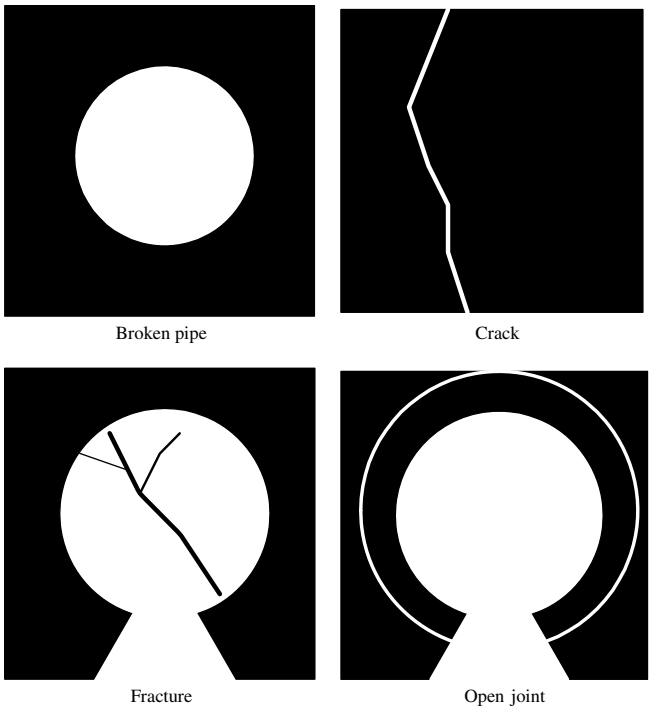

Fig. 6. Ideal morphologies of pipe defects.

morphology segmentation of these two patterns of pipe defects. A slight crack was segmented into two or more white image regions in the segmented binary images C1 and C5, so an approach of edge linking should be employed to link the separated white image regions to display a complete segmented crack. Unfortunately, some slight crack, such as that shown on the gray-level CCTV image C2 whose top is obviously lighter than its bottom, could not be effectively segmented due to the unequal light sourcing. In conclusion of the above discussions about segmentation failure, most of the pipe defects on CCTV images can not be segmented completely due to the camera pose, light sourcing, notations on CCTV images, sewages within pipes, or other factors.

The binary images, B4, C5, F1, and O5 in Fig. 5, are the examples on which the morphologies of pipe defects were segmented successfully. Among the 291 samples of pipe defects acquired, there were 62 samples of pipe defects including 5, 22, 2, and 33 samples of broken pipe, crack, fracture, and open joints, respectively, segmented successfully. Because fracture has many failure cases of segmentation, this paper employs the other 60 pipe defects segmented successfully for diagnosis of pipe defects. The morphological features of the 60 pipe defects are listed in Table 1. Obviously, the areas of broken pipe or open joint are much larger than those of cracks. The eccentricities of broken pipe range from 0.6 through 0.8; those of crack are almost above 0.9, and those of open joint almost range from 0.3 through 0.6. As for the ratio of major axis length to minor, those of broken pipe or open joint range from 1.0 through 2.0, but those of cracks due to its long and narrow

Table 1
Morphological features of successfully segmented pipe defects

Pipe defects	Area	Major axis length	Minor axis length	Eccentricity	Major/minor
Broken pipe	11025	179.3331	129.7225	0.6905	1.3824
	10662	155.0269	105.2767	0.7341	1.4726
	8934	145.9232	103.9595	0.7017	1.4037
	10941	171.1512	106.1450	0.7845	1.6124
	5379	96.3136	73.8643	0.6417	1.3039
Crack	907	97.8161	14.2119	0.9894	6.8827
	2182	141.1859	111.7988	0.6107	1.2629
	1904	152.8344	24.5892	0.9870	6.2155
	841	155.2565	8.7959	0.9984	17.6510
	318	158.3682	11.6273	0.9973	13.6204
	83	42.6751	6.1486	0.9896	6.9406
	558	153.9083	20.6073	0.9910	7.4686
	104	99.8998	6.9348	0.9976	14.4056
	438	43.6900	17.4418	0.9169	2.5049
	202	96.3043	8.0486	0.9965	11.9654
	69	40.0425	4.7486	0.9929	8.4325
	60	39.6009	8.1370	0.9787	4.8668
	72	66.3502	4.7615	0.9974	13.9347
	206	111.1348	11.1307	0.9950	9.9845
	258	137.0497	11.2996	0.9966	12.1287
	126	75.7388	4.8499	0.9979	15.6166
	57	33.0237	2.6561	0.9968	12.4331
	325	144.7255	13.7188	0.9955	10.5494
	419	170.1375	19.9687	0.9931	8.5202
	417	138.6845	20.2706	0.9893	6.8417
	169	94.5528	5.5906	0.9983	16.9128
	83	69.8607	3.5234	0.9987	19.8276
Open joint	4680	165.3972	69.1441	0.9084	2.3921
	9667	130.3706	126.2636	0.2490	1.0325
	9831	130.7117	117.5811	0.4368	1.1117
	7005	109.6634	94.9257	0.5007	1.1553
	14074	163.5757	132.9916	0.5822	1.2300
	7597	151.4679	90.9738	0.7995	1.6650
	12316	167.5232	148.3640	0.4644	1.1291
	10887	147.1307	134.4684	0.4059	1.0942
	13754	172.2098	150.0235	0.4910	1.1479
	9264	148.2113	121.7512	0.5703	1.2173
	12481	163.8687	135.0470	0.5664	1.2134
	11139	147.4967	139.6121	0.3226	1.0565
	6465	110.1912	90.9229	0.5649	1.2119
	8029	128.4295	107.9100	0.5422	1.1901
	9157	138.3897	113.7347	0.5697	1.2168
	8766	129.6492	116.0195	0.4463	1.1175
	8447	140.5758	109.1084	0.6305	1.2884
	7098	128.5467	101.0536	0.6181	1.2721
	9601	154.0402	111.4404	0.6904	1.3823
	7525	151.7261	98.1155	0.7628	1.5464
	8279	140.3253	115.9082	0.5637	1.2107
	9425	139.6398	128.2848	0.3950	1.0885
	12058	174.6893	136.2170	0.6261	1.2824
	8746	136.3048	129.3318	0.3157	1.0539
	6840	154.7491	127.4175	0.5675	1.2145
	9563	141.4691	120.8469	0.5199	1.1706
	11849	154.5819	133.8950	0.4997	1.1545
	11183	174.9488	146.4154	0.5473	1.1949
	10757	177.8374	155.2148	0.4881	1.1458
	8248	163.0742	138.4349	0.5285	1.1780
	9455	149.0819	130.7129	0.4809	1.1405
	14889	167.2766	137.2068	0.5720	1.2192
	14206	148.5983	141.2652	0.3103	1.0519

shape are much larger than those of broken pipe or open joint.

4.4. Diagnosis of pipe defects

To train the diagnostic system, two experiments (I and II) were given by 15 and 30 pipe defects, which were randomly selected from the 60 pipe defects and implemented an expertise-based human diagnosis a priori, respectively. Also, the assignment of training samples saved three quarters and a half of expertise-based human diagnosis in Experiments I and II, respectively. Regarding to Table 1, the proportions of broken pipe, cracks, and open joint are 8.3%, 36.7%, and 55.0%, respectively. Assuming unequal prior probability, in Experiment I the frames of training images of broken pipe, cracks, and open joint were given by 1, 6, and 8, respectively; in Experiment II the frames of training images of broken pipe, cracks, and open joint were given by 2, 11, and 17, respectively. Under the different assignment of training image numbers, both the accuracy and efficiency of the diagnostic system are assessed.

Table 1 shows that the original morphological features of pipe defects is a five-dimensional set of data. Before inputting the morphological features of pipe defects into the diagnostic system, the five-dimensional set of data was transformed by PCA into a two-dimensional set of uncorrelated variables representing about 95% information (see Table 2). This two-dimensional set of uncorrelated variables was analyzed by the diagnostic system and obtained training accuracies of 100.0% for both Experiments I and II as well as overall accuracies of 93.3% and 95.0%, respectively (see Tables 3 and 4). Due to the insignificant improvement of the overall accuracy in Experiment II comparative to Experiment I, the assignment of training samples in Experiment I is adequate for the automated diagnosis of pipe defects.

In addition to the overall accuracy, both of Tables 3 and 4 also list producer's accuracies and user's accuracies. Producer's accuracies result from dividing the number of correctly classified pipe defects in each category (on the major diagonal) by the number of training set pipe defects used for that category (the column total); user's accuracies are computed by dividing the number of correctly classified pipe defects in each category by the total number of pipe defects that were classified in that category (the row total) (Lillesand & Kiefer, 2000). The proposed diagnostic system can distinguish open joint exactly, whereas it just offers a user's accuracy of about 90%. On the contrary, both the user's accuracies of broken pipe and cracks are 100%. However, broken pipe comparative to cracks has a greater probability to be misdiagnosed into open joint due to its relative less number of training samples. The acceptable overall accuracy of above 90% demonstrates that the defined morphological features of pipe defects have a well discriminant and will be useful in the further applications of diagnosis of pipe defects.

Table 2
Proportion of trace explained

Principal component	Variance	Cumulative variance
1	0.875	0.875
2	0.077	**0.952**
3	0.025	0.977
4	0.018	0.995
5	0.005	1.000

Table 3
Classification matrix of sewer pipe defects in Experiment I (15 training samples)

Classification data	Reference data			
	Broken pipe	Crack	Open joint	Row total
Broken pipe	2	0	0	2
Crack	0	21	0	21
Open joint	3	1	33	37
Column total	5	22	33	60
Producer's accuracy			User's accuracy	
Broken pipe = 40.0% (2/5)			Broken pipe = 100.0% (2/2)	
Crack = 95.5% (21/22)			Crack = 100.0% (21/21)	
Open joint = 100.0% (33/33)			Open joint = 89.2% (33/37)	
Overall accuracy = 93.3%				

Table 4
Classification matrix of sewer pipe defects in Experiment II (30 training samples)

Classification data	Reference data			
	Broken pipe	Crack	Open joint	Row total
Broken pipe	3	0	0	3
Crack	0	21	0	21
Open joint	2	1	33	36
Column total	5	22	33	60
Producer's accuracy			User's accuracy	
Broken pipe = 60.0% (3/5)			Broken pipe = 100.0% (3/3)	
Crack = 95.5% (21/22)			Crack = 100.0% (21/21)	
Open joint = 100.0% (33/33)			Open joint = 91.7% (33/36)	
Overall accuracy = 95.0%				

5. Conclusions and suggestions

Several automated diagnostic systems based on the morphological features of pipe defects have been developed in literature, but the systems still need an expertise-based human diagnosis to identify the image regions of pipe defects from a segmented binary image for the automated diagnosis. In order to reduce human effort for automation, firstly a combination of opening operation and Otsu's technique was used for segmenting the morphologies of pipe defects including broken pipe, cracks, fracture, and open joint in this paper. Especially, opening operation with a disk structuring element of radius $r = 4$ is useful for mostly smoothing the notations of inspection attributes manually recorded on CCTV images with the shapes of pipe defects effectively remained. However, it is found that the combi-

nation of opening operation and Otsu's technique for segmenting the morphologies of pipe defects is still affected by camera pose, light sourcing, sewages within pipes, notations unsmoothed thoroughly, or other factors. If a camera pose is not adjusted to shoot an approximately flat object such as the CCTV image C5 in Fig. 2, basically light sourcing can not be uniformly distributed on the CCTV image so that the morphology of the pipe defect on the CCTV image can not be effectively segmented.

Based on the segmentation results in this research, the ideal morphologies of the four types of pipe defects on CCTV images were defined (see Fig. 6). Among the 291 samples of pipe defects acquired, 62 samples were segmented successfully to be measured their morphological features. In this paper, the ideal morphology segmentation of pipe defects did not be used for diagnosis of fracture pipe defects due to its high percentage of segmentation failure. The other 60 success samples including 5, 22, and 33 samples of broken pipe, crack, and open joints, respectively, were used for the automated diagnosis of pipe defects. There were two experiments (I and II), in which 15 and 30 training samples were given, respectively, designed to assess the accuracy and efficiency of the diagnostic system. The experimental results reveal that the overall accuracies of Experiments I and II are 93.3% and 95.0%, respectively. Due to the insignificant improvement of the overall accuracy in Experiment II comparative to Experiment I, assigning a quarter of all data as training samples is adequate for the automated diagnosis of pipe defects that saved the human effort on diagnosing the rest three quarters of CCTV images. To obtain more CCTV images with ideal morphology segmentation of pipe defects, we suggest that a regulation for camera pose and light source should be systematically established in the further inspection works by referring to the CCTV images segmented successfully, such as B4, C5, F1, and O5 in Fig. 2. In addition, the notations of inspection attributes should be recorded in a separate management system rather than direct on CCTV images so to avoid interfering optimal thresholds while using Otsu's technique to segment the morphologies of pipe defects.

Acknowledgements

This study was sponsored by the Construction Bureau, Construction and Planning Agency, Ministry of the Interior, Taiwan. Also, the Taichung City Government is appreciated for offering the CCTV images.

Appendix

Area = area of pipe defect in pixels;
major axis length = length of the major axis of the "area" refer to above;
minor axis length = length of the minor axis of the "area" refer to above;
eccentricity = ratio of the distance between foci of ellipse and its major axis length;
ratio of major axis length to minor = major axis length (as defined in this Appendix)/minor axis length (as defined in this Appendix).

References

Dong, P. (1997). Implementation of mathematical morphological operations for spatial data processing. *Computers & Geosciences, 23*(1), 103–107.

Duda, R. O., Hart, P. E., & Stork, D. G. (2001). *Pattern classification*. New York: Wiley.

Fenner, R. A. (2000). Approaches to sewer maintenance: A review. *Urban Water, 2*(4), 343–356.

Gokhale, S., & Graham, J. A. (2004). A new development in locating leaks in sanitary sewers. *Tunnelling and Underground Space Technology, 19*(1), 85–96.

Gonzalez, R. C., & Woods, R. E. (2002). *Digital image processing* (2nd ed.). New Jersey: Prentice Hall.

Han, M., & Xi, J. (2004). Efficient clustering of radial basis perceptron neural network for pattern recognition. *Pattern Recognition, 37*(10), 2059–2067.

Hwang, Y. S., & Bang, S. Y. (1997). Recognition of unconstrained handwritten numerals by a radial basis function neural network classifier. *Pattern Recognition Letters, 18*(7), 657–664.

Iyer, S., & Sinha, S. K. (2005). A robust approach for automatic detection and segmentation of cracks in underground pipeline images. *Image and Vision Computing, 23*(10), 921–933.

Jang, B. K., & Chin, R. T. (1998). Morphological scale space for 2D shape smoothing. *Computer Vision and Image Understanding, 70*(2), 121–141.

Liao, Y., Fang, S. C., & Nuttle, H. L. W. (2004). A neural network model with bounded-weights for pattern classification. *Computers and Operations Research, 31*(9), 1411–1426.

Lillesand, T. M., & Kiefer, R. W. (2000). *Remote sensing and image interpretation* (4th ed.). New York: Wiley.

Makar, J. M. (1999). Diagnostic techniques for sewer systems. *Journal of Infrastructure Systems, 5*(2), 69–78.

Mckim, R. A., & Sinha, S. K. (1999). Condition assessment of underground sewer pipes using a modified digital image processing paradigm. *Tunneling and Underground Space Technology, 14*(2), 29–37.

Moselhi, O., & Shehab-Eldeen, T. (1999). Automated detection of surface defects in water and sewer pipes. *Automation in Construction, 8*(5), 581–588.

Moselhi, O., & Shehab-Eldeen, T. (2000). Classification of defects in sewer pipes using neural network. *Journal of Infrastructure Systems, 6*(3), 97–104.

Parker, J. R. (1997). *Algorithms for image processing and computer vision*. New York: John Wiley & Sons, Inc.

Polat, K., & Güneş, S. (2007). Automatic determination of diseases related to lymph system from lymphography data using principles component analysis (PCA), fuzzy weighting pre-processing and ANFIS. *Expert Systems with Applications, 33*(3), 636–641.

Seo, K. K. (2007). An application of one-class support vector machines in content-based image retrieval. *Expert Systems with Applications, 33*(2), 491–498.

Shehab, T., & Moselhi, O. (2005). Automated detection and classification of infiltration in sewer pipes. *Journal of Infrastructure Systems, 11*(3), 165–171.

Sinha, S. K., & Fieguth, P. W. (2006). Segmentation of buried concrete pipe images. *Automation in Construction, 15*(1), 47–57.

Wang, X., & Paliwal, K. K. (2003). Feature extraction and dimensionality reduction algorithms and their applications in vowel recognition,

Pergamon. *The Journal of the Pattern Recognition Society, 36*, 2429–2439.

Water Research Centre (1994). Sewerage rehabilitation manual (3rd ed.). Swindon, UK: Water Research Centre/Water Authorities Association.

Widodo, A., Yang, B. S., & Han, T. (2007). Combination of independent component analysis and support vector machines for intelligent faults diagnosis of induction motors. *Expert Systems with Applications, 32*(2), 299–312.

Wirahadikusumah, R., Abraham, D. M., Iseley, T., & Prasanth, R. K. (1998). Assessment technologies for sewer system rehabilitation. *Automation in Construction, 7*(4), 259–270.

Yan, H. (1996). Unified formulation of a class of image thresholding techniques. *Pattern Recognition, 29*(12), 2025–2032.

Yang, M. D., & Su, T. C. (2006). An automation model of sewerage rehabilitation planning. *Water Science and Technology, 54*(11–12), 225–232.

Yang, M. D., & Su, T. C. (2007). An optimization model of sewage rehabilitation. *Journal of the Chinese Institute of Engineers, 30*(4), 651–659.

Yang, M. D., & Su, T. C. (2008). Automated diagnosis of sewer pipe defects based on machine learning approaches. *Expert Systems with Applications., 35*(3), 1327–1337.

Zhang, C., Jiang, J., & Kamel, M. (2005). Intrusion detection using hierarchical neural networks. *Pattern Recognition Letters, 26*(6), 779–791.